Qualitative analysis of Zircaloy-4 cladding air degradation in O2-N2 mixtures at high temperature

Marina Lasserre, Véronique Peres, Michèle Pijolat, Olivia Coindreau, Christian Duriez, Jean Paul Mardon

Qualitative analysis of Zircaloy-4 cladding air degradation in O_2-N_2 mixtures at high temperature

M. Lasserre [1,2,*], V. Peres [2], M. Pijolat [2], O. Coindreau[1], C. Duriez[1], J.-P. Mardon [3]

[1] Institut de Radioprotection et de Sûreté Nucléaire, Cadarache Center, France

[2] Ecole Nationale Supérieure des Mines, SPIN, PRESSIC, CNRS:UMR-5307 LGF, F-42023 Saint-Etienne, France

[3] AREVA, AREVA NP Fuel Business Unit, Lyon, France

[*] IRSN, PSN-RES/SAG/LESAM Bat 700, 13115 Saint Paul lez Durance Cedex, France

Email: M. Lasserre (marina.lasserre@irsn.fr)

Keywords: Zircaloy-4; thermogravimetry; high temperature corrosion; oxygen-nitrogen mixture atmospheres

Abstract

This article is devoted to the qualitative analysis of the Zircaloy-4 degradation mechanism at 850°C in oxygen/ nitrogen partial pressure atmospheres. Thermogravimetry, optical microscopy, scanning electron microscopy and energy dispersive X-ray spectrometry, are used to provide some information regarding the oxidation kinetics and the various phases involved along the process. The kinetic curves reveal two stages: a pre-transition and a post-transition one. Oxide growth during the pre-transition stage is controlled by oxygen vacancy diffusion in the oxide layer, since neither oxygen nor nitrogen partial pressure influences the kinetics. In the post-transition stage, nitrogen has an accelerating effect in the corrosion reaction. The kinetic curves reveal two distinct behaviours after the transition according to the oxygen and nitrogen partial pressures: in the first case the corrosion rate rises substantially and leads to a rapid degradation of the metal at high oxygen and nitrogen partial pressures, in the second case the corrosion rate rises dramatically and reaches a plateau at low oxygen and nitrogen partial pressures. This paper describes the influence of both gases on the corrosion kinetics in relation with morphological observations, analyses the discrepancies found between high and low oxygen and nitrogen partial pressures; it also exhibits the

complexity of the solid state transformations due to three distinct reactions that appear to take place during the corrosion process.

1 Introduction

The understanding of Zircaloy-4 (Zry-4) cladding behaviour during high temperature air ingress situations is of primary importance for some nuclear accidental situations. Indeed, in case of a severe accident in a nuclear power plant, such as a loss of water from a spent fuel pool, in case of a degraded transport situations or a core meltdown accident with subsequent reactor pressure vessel failure, Zry-4 cladding, providing the first containment of UO_2 fuel, could be exposed to air. Due to the lack of fuel assemblies cooling, temperature increases significantly. As a result, accelerated corrosion of the Zry-4 claddings takes place, which leads to their strong degradation and the release of fission products; some of them being highly radiotoxic and potentially harmful to the population and environment.

The purpose of researches made in this field is to implement a model witch could represent what happens in air ingress situations and consequently to better anticipate consequences and circumstances of such accidents [1].

It is clear that during accidental situations, Zry-4 is not only exposed to air but also to radiations, steam atmosphere, temperature and partial pressure transients. In addition, during its use in PWR (Pressurized Water Reactor), the cladding has been first pre-oxidised and submitted to numerous stresses such as neutron flux, formation of new radioactive species due to fission reactions, mechanical, chemical, hydraulic and last but not least thermal stresses. Obviously, all these factors have to be taken into account during high temperature air ingress modelling and currently, some of them are experimentally investigated in recent studies by means of separated effect tests [2-6]. Nevertheless, as little information is available concerning the high temperature degradation mechanism of Zry-4 cladding in mixed oxygen and nitrogen atmospheres, this remains an area that requires further investigations. That is the reason why the present work addresses this problem and presents the difficulties encountered to express the reaction rate not only regarding the various transformations of the metal that could happen during the corrosion process, but concerning influence of both nitrogen and oxygen partial pressures on the reaction rate as well.

This paper presents first a brief state of knowledge concerning behaviour of zirconium alloy during air ingress situations. Then, experimental details, relating to the sample preparations and the

thermogravimetric apparatus, are described. Finally, experimental results obtained with thermogravimetric tests are presented and discussed in order to underline the influence of partial pressures on the reaction rate and the complexity of nitrogen attack.

2 State of knowledge

Considering the Gibbs energy of formation of ZrO_2 and ZrN (zirconium nitride),ZrO_2 formation is clearly energetically more favourable than ZrN formation as long as oxygen remains in the atmosphere. At 850°C, $\Delta_r G_O^0(1123) = -887.7$ kJ.mol^{-1} and $\Delta_r G_N^0(1123) = -259.9$ kJ.mol^{-1}.

From equations (1) and (2), it can be calculated that at 850°C, formation of ZrO_2 and ZrN for each reaction separately is favourable above oxygen and nitrogen equivalent partial pressures of $p_{O2} = 5.09.10^{-42}$ atm and $p_{N2} = 6.66.10^{-25}$ atm respectively.

$$\Delta_r G_O^0 = -RT\ln K = RT\ln\left(\frac{p_{O2}}{p_0}\right) \quad (1)$$

$$\Delta_r G_N^0 = -RT\ln K = RT\ln\left(\frac{p_{N2}}{p_0}\right)^{1/2} \quad (2)$$

Fig. 1 shows the stability diagram of Zr, ZrN and ZrO_2 phases at 850°C for different oxygen and nitrogen equivalent partial pressures. Due to the very low oxygen pressure at Zr/ZrO_2 equilibrium ($p_{O2} = 5.09.10^{-42}$ atm), when considering first formation of ZrO_2 and secondly, incorporation of nitrogen into the oxide layer, formation of ZrN is possible near the metal-oxide interface at very low equivalent nitrogen partial pressures ($p_{N2} > 6.66.10^{-25}$ atm).

Previous studies have shown that the presence of both nitrogen and oxygen in the atmosphere significantly increases corrosion kinetic rate of Zry-4 cladding compared with free oxygen or free steam atmospheres [7-10]. This phenomenon appears to be related to the nitrogen attack, producing zirconium nitride precipitates and a highly porous oxide layer. Two distinct interpretations have been suggested to explain the formation of zirconium nitride precipitates.

The first one is related to oxygen partial pressure knowing that, during air corrosion of Zry-4, the reaction with oxygen is preferred to that with nitrogen. According to Duriez and Steinbrück [2-4], nitriding and fast degradation of Zry-4 cladding can be described according to the following sequence of events:

- a dense oxide forms first; while its thickness grows, compressive stresses in the oxide build up and are released by formation of cracks, giving direct access of air to the metal,
- oxygen is consumed first at the bottom of the cracks, creating here a microscopic oxygen starvation (lack of oxygen in the atmosphere). Then, nitrogen reacts with the α-Zr(O) phase, which is present between ZrO_2 and Zry-4 phases, or the sub-stoichiometric oxide. As the reaction proceeds, the oxygen-nitrogen stabilized α phase converts to a ZrO_2-ZrN two-phase mixture when the solubility limit is exceeded. This reaction creates pores, which are preferentially located along the ZrN precipitates with the highest density [11],
- as the oxide scale grows inward, the zirconium nitride formed is oxidised by fresh air flowing near the external surface. Due to the lower density of ZrO_2 in comparison to ZrN, this reaction is followed by a volume increase leading to the formation of microcracks and giving direct access for the air to the metal.

According to other studies, dissolution of nitrogen into zirconia would be another possibility to describe zirconium nitride formation near the oxide-metal interface [8, 9, 12]. Nitrogen incorporation into zirconia lattice can be expressed according to the following reaction [13-15]:

$$3O_O^X + N_2 = 2N'_O + V_O^{\bullet\bullet} + 3/2\ O_2 \qquad (3)$$

Due to charge equilibrium two nitrogen anions replace three oxygen anions on the regular oxygen sites of the zirconia anionic sublattice. This phenomenon creates an oxygen vacancy in the anionic sublattice and the release of gaseous oxygen. Presence of oxygen vacancies in the zirconia anionic sublattice has an effect on the stability of tetragonal and cubic phases of zirconia [16-19]. Depending on the amount of nitrogen in the oxide solid solution various phases of zirconium oxynitride may precipitate [20-24], namely ß'-$Zr_7O_{11}N_2$, ß''-$Zr_7O_{9,5}N_3$, ß- $Zr_7O_8N_4$ and γ-Zr_2ON_2. When the local thermodynamic conditions are favourable, zirconium nitride Zr_3N_4 is formed. On heating in nitrogen, Zr_3N_4 decomposes above 1100K into ZrN and N_2. In air, it starts to oxidise at 800K [25].

It is necessary to deeper investigate the corrosion process in O_2-N_2 mixtures in order to confirm or not both previous interpretations. So the choice has been done to follow the kinetics using small thin plates in order to maintain constant the gas partial pressures along the entire sample surface and to study the influence of O_2 and N_2 composition on the overall process.

3 Experimental

3.1 Sample

Specimens coming from a standard 0.45 mm sheet of recrystallized Zry-4 provided by Areva NP were cut to 10mm x 10mm for the corrosion tests. The chemical composition of the investigated alloy is shown in the table below. The bare samples were cleaned with acetone and dried.

Composition of the Zry-4 alloy

Alloy	Sn (wt. %)	Fe (wt. %)	O (wt. %)	Cr (wt. %)	C (wt. ppm)	Nb (wt. ppm)	H (wt. ppm)
Zircaloy-4	1.32-1.35	0.21	0.123-0.129	0.11	125-140	<40	<3

3.2 Thermogravimetric apparatus

The corrosion kinetics in O_2/N_2/He or Ar flowing mixtures (flow rate in one furnace is 5 $L.h^{-1}$) was followed by means of a symmetrical microbalance (Sétaram TAG-24) equipped with a thermoregulated cooling fluid. While the sample was suspended to an alumina rod, a specific alumina plate sample had been designed and placed in the reference furnace in order to minimise baseline shift during experiments. Partial pressures of O_2 and N_2 were adjusted to the desired values by mass flow meters.

All the corrosion tests were conducted at 850°C after a heating ramp of 10°C.min^{-1} in the desired gas mixture. In a first series of experiments the oxidant gas was a 20% O_2 - 80% N_2 mixture. In a second series, the samples were oxidized in 5% O_2 - 5% N_2 – 90% He. A third series of oxidation tests was done first under 20% O_2 - 80% N_2 during various period, then the gas flow rate was switched to argon.

3.3 Characterization methods

Optical microscopy, scanning electron microscopy (SEM) and energy dispersive X-ray spectrometry with silicon drift detector (EDX-SDD) were used for morphological observations.

Corroded samples were cold embedded in resin 605 (methyl methacrylate) and polished with MECAPOL P320 PRESI device. Polishing was performed with ceramic papers and diamond pastes. For SEM and EDX-SDD analyses a fine carbon deposit was put on the surface of the samples.

4 Experimental results and discussions

4.1 Corrosion in 20% O_2 - 80% N_2 of Zry-4 at 850°C

Fig. 2A shows the mass gain curve in $mg.cm^{-2}$ as a function of time during an experiment in 20% O_2 - 80% N_2. The corresponding rate of mass gain curve is shown in Fig. 2B. It can be seen from Fig. 2A that the mass gain reached at the beginning of the plateau is only 0.03% of the total mass gain after

6 hours at 850°C. The initial rate increase in Fig. 2B corresponds to the temperature increase up to 850°C, then the rate decreases, which corresponds to the "pre-transition stage" during which the oxide growth kinetics is known to be controlled by oxygen vacancy diffusion through a dense zirconia layer. This is the reason why, Duriez et al. [2] reported that the kinetic rate follows a parabolic law during the pre-transition stage where the rate-limiting step is the diffusion in the oxide layer of oxygen vacancies that are created at the internal interface. In addition, these authors have shown that the parabolic rate constants obtained during corrosion in air for different temperatures are close to those obtained during oxidation of Zry-4 or corrosion in steam. Then, the rate passes through a minimum corresponding to a "kinetic transition" whose the origin, which has been the subject of many discussions in the past [10, 26]. This transition is usually associated to the formation of first cracks in the dense zirconia layer. During the "post transition" stage, cracks in the oxide layer, which is no longer protective, spread over the surface of the sample allowing gas phase diffusion into the cracked oxide scale. The accelerating effect of nitrogen on the kinetics is observable in Fig. 2B where the kinetic rate obtained under 20% O_2 - 80% He is found to be much lower than that under 20% O_2 - 80% N_2, for which there is a very important increase of the kinetic rate during the post-transition stage.

Fig. 3 represents the kinetic curves of mass gain (Fig. 3A) and rate of mass gain (Fig. 3B) versus time obtained in experiments performed under the same conditions in order to appreciate their reproducibility. It can be seen that if the curves are very well superimposed up to the kinetic transition then, scattering of the TGA traces after the transition is high during the post-transition stage.

For same experimental conditions the temperature program was shortened in order to observe the morphological changes corresponding to the pre-transition stage (Fig. 4A), the kinetic transition (Fig. 4B) and the post-transition stage (Fig. 4C) by optical and SEM microscopy.

During the pre-transition stage (Fig. 4A), the protective oxide layer ZrO_2 is dense and adherent to the metal. Its thickness is about 9 μm for a mass gain of 1.76 $mg.cm^{-2}$. We can notice that zirconium nitride precipitates, whose colour is gold in optical microscopy and white (the clearest regions in the corroded zone) in SEM, are clearly visible at metal-oxide interface and sometimes inside the protective oxide layer itself. In addition, we can see some cracks along the oxide layer although the kinetic transition is still not yet reached.

The kinetic transition observed during corrosion in air is still a phenomenon that arises considerable interest and attention. Indeed, many assumptions have been made regarding breakaway activation [10, 26], which could be mechanical-type (release of compressive stresses) or chemical-type (tetragonal to monoclinic zirconia phase transformation). However, these assumptions do not explain why, in the presence of nitrogen in the gaseous phase, first cracks appear significantly earlier than during oxidation under oxygen alone. This could be due to the fact that formation of zirconium nitride precipitates during the pre-transition stage has an influence on the breakaway activation and so, on the kinetic rate. According to Evans et al., who studied the effect of nitrogen on Zr metal exposed to O_2-N_2 mixtures [8], the breakaway activation could be induced by the oxidation of zirconium nitride particles formed during the pre-transition stage. Our observations clearly support that interpretation.

Microviews of the sample at the kinetic transition can be seen in Fig. 4B. We can notice that the kinetic transition takes place first on the edges of the plate. In addition, the corroded regions are characterized by large cracks perpendicular to the dense zirconia layer formed during the pre-transition stage. Directly beneath the cracked oxide layer, the scale is porous and exhibits cracks parallel to the surface sample. Moreover, there are some zirconium nitride precipitates near to the metal-oxide interface together with regions of dense zirconia in contact with the metal. This latter observation is much more visible in Fig. 4C, which corresponds to samples in the post-transition stage.

During the post-transition stage, curves of Fig. 3B clearly show a drastic rise of the kinetic rate. When we look at the global morphological changes of the sample during post-transition stage (Fig. 4C), we can see that the breakaway activation is a non-uniform process. Hence, the kinetic transition does not occur at the same time on the whole oxide layer. By this fact, the mass gain is the result of two contributions: one is due to the dense zirconia growth corresponding to the pre-transition regions, whereas the other is due to the regions that have already passed the kinetic transition. Moreover, whereas the oxide growth in the pre-transition regions is parallel to the initial surface plane, the post-transition regions progress in an isotropic way, which leads to a half-ellipsoïdal shape of each corroded zone. From a phenomenological point of view, the kinetic model best adapted to describe such behaviour is a surface nucleation and growth model according to

Mampel's assumptions [27, 28], which was initially used to describe the kinetics of thermal transformations of powders.

A comprehensive description of the kinetic transition appearing during Zry-4 oxidation (without nitrogen) based on Mampel's model can be found in [1, 26, 29]. Similar mathematical calculations could be applied to explain the shape of the kinetic curves under a 20% O_2 – 80% N_2 mixture assuming that (i) the post-transition regions (large cracks zones) appear at random at the sample surface just as nuclei with a nucleation frequency depending on temperature, oxygen and nitrogen partial pressures (this will be discussed later in section 4.2), alloy composition, etc.; and (ii) the growth kinetics of these nuclei is controlled by an interfacial reaction where the nitrogen containing phases are probably involved.

In order to better characterize the regions containing the nitride precipitates, a sample corresponding to the post-transition stage (see Fig. 4C, mass-gain: 15.76 $mg.cm^{-2}$), has been analysed by energy dispersive X-ray spectrometry with silicon drift detector (EDX-SDD). The micrograph and the corresponding EDX spectrum are shown in Fig. 5.

The carbon peak on the X-ray diffractogram is due to the carbon layer deposit put on the surface of the sample for the observation. Fig. 5 shows that the analysed regions (9, 10,11 and 12) of the corroded sample in the SEM views seem to contain both oxygen and nitrogen elements. They could thus be either a ZrO_2-ZrN two-phase mixture or Zr_2ON_2 zirconium oxynitride whose colour in optical microscopy is closed to that of Zr_3N_4 [30]. Based on the assumption that the clearest regions of the corroded sample are zirconium oxynitride precipitates, several hypotheses could be made concerning their origin. Indeed, the formation of zirconium oxynitride precipitates could result from nitrogen dissolution in zirconia up to the solubility limit (as previous mentioned in section 2) or from the oxidation of zirconium nitride during the cooling subsequently to the 850°C plateau. In addition, oxidation of the sample surface during EDX-SDD measurement cannot be excluded, which could have distorted the results.

4.2 Influence of O_2 and N_2 partial pressures on the corrosion behaviour

Series of experiments have been performed at 850°C in various conditions of oxygen and nitrogen partial pressures.

As revealed by the kinetic curves presented in Fig. 6, when the sample are corroded in 5% O_2 - 5% N_2 – 90% He atmosphere, the kinetic rate after the kinetic transition first increases and finally reaches

a constant value which is more or less the same for all experiments (0.00245 ± 0.00015 mg.cm^{-2}.s^{-1}). Moreover, it clearly appears that the reproducibility in the low partial pressures conditions is better than in the 20% O_2 – 80% N_2 mixture, showing that the processes involved here are probably more controlled by thermodynamic conditions, since the experimental device and the sample preparations are identical to those previously reported (section 3.2).

Fig. 7 shows a comparison between kinetic curves obtained in three different conditions: 5% O_2 - 5% N_2 – 90% He, 10% O_2 - 20% N_2 – 70% He and 20% O_2 - 80% N_2. Despite the non-reproducibility aspects already discussed, it appears that the decrease in both nitrogen and oxygen partial pressures significantly modifies the shape of the kinetic curves (clearly visible in Fig. 7B) by increasing the mass gain rate after kinetic transition and lowering it at the end of the plateau. Such effects could result from differences in the initiation (nucleation) and propagation (growth) of corroded regions in the post-transition stage.

Images obtained by optical metallography of samples corroded in 5% O_2 - 5% N_2 – 90% He atmosphere up to various mass gains during the post-transition stage are shown in Fig. 8A (5 mg.cm^{-2}, i.e. just after the kinetic transition), Fig. 8B (10.2 mg.cm^{-2}, i.e. during the kinetic acceleration) and Fig. 8C (35 mg.cm^{-2}, i.e. when the kinetic rate is constant).

As the transformation proceeds, the kinetic transition takes place first on the edges of the sample (Fig. 8A) then spreads over the whole surface of the sample (Fig. 8B). When the kinetic rate become constant versus time, we see that the whole sample is in post-transition stage (Fig. 8C). Moreover, we can see in Fig. 8A and Fig. 8B that small zirconium nitride precipitates (or zirconium oxynitride precipitates, according to results proposed in section 4.1) are uniformly spread at the metal-oxide interface.

The most striking feature that can be deduced from these observations is the uniformity of the post-transition regions along the whole sample surface contrarily to the localized attacks seen in 20% O_2 - 80% N_2 conditions. It comes out that the oxygen and nitrogen partial pressures play an important role on the initiation process of the kinetic transition, i.e. the nucleation process as previously discussed in section 4.1 is greatly dependant on the oxygen and nitrogen partial pressures; thus, according to the oxygen and nitrogen composition, the global kinetic rate, which depends of both nucleation and growth processes, varies differently versus time and if the number of nuclei per unit of time and surface area is high in the 5% O_2 - 5% N_2 – 90% He mixture, the surface of the sample is

rapidly covered with post-transition regions, leading to a continuous corroded layer as seen in Fig. 8C. Moreover, the fact that, at low oxygen and nitrogen partial pressures, the kinetic rate reaches a constant value is in total agreement with a uniformly corroded sample since it is known (from the nucleation and growth models) that the acceleration period in the kinetic curves is due to the growth of the various nuclei that appear at different times of the transformation.

4.3 Understanding of the role of nitrogen on the accelerated corrosion

Some tests have been performed in order to better understand the role of nitrogen on the corrosion acceleration, and especially the nature of the chemical reactions involved between the various phases observed in the sample. The principle of these tests consists in first exposing the sample to "normal" conditions of corrosion as those described in section 4.1 (20% O_2 - 80% N_2) and then switching the gas flow to inert gas (Ar or He). By using this procedure, starvation conditions take place and only nitrogen located at the metal-oxide interface, i.e. formed during normal conditions of corrosion, reacts. This separate effect test could give some information concerning nitrogen attack once precipitates are formed and so, could allow better understanding why transition occurs and what sequence of events happens during post-transition stage.

Results presented hereafter have been obtained by switching from the reactant mixture to the inert atmosphere at various mass gains after the kinetic transition as indicated by the arrows on Fig. 9, which represents the kinetic curves measured at 850°C. After switching to the inert atmosphere, a very little increase in mass gain still occurs (0.55 $mg.cm^{-2}$ after 3 hours), due to oxygen traces contained in flowing argon (31 ppm O_2).

From the images obtained by optical metallography and SEM (see Fig. 10A, Fig. 10B, Fig. 10C), we can clearly see that, for each sample, there are many voids located in the metal side just in the vicinity of the gold coloured precipitates. These voids can be explained by the outward growth of a zirconium-rich phase such as the nitride (or oxynitride) phase due to reaction between nitrogen and metallic zirconium (in fact the α-Zr(O) phase). Observations during Zry-4 corrosion in 5% O_2 -5% N_2 – 90% He, before switching to inert atmosphere, lead to the same conclusions than in 20% O_2 - 80% N_2. So, these experiments indicate that, in oxygen starvation conditions, nitrogen may react with the metal according to an outward growth to form zirconium nitride (or/and zirconium oxynitride) precipitates, i.e. in the direction of the gas/oxide interface.

From the various results presented in section 4, the following sequence may be proposed in order to describe the corrosion process of Zry-4 in oxygen and nitrogen mixtures at 850°C:

- in the first period usually called the pre-transition stage, nitrogen is incorporated in sub-stoichiometric zirconia forming a solid solution whereas the kinetic rate decrease corresponds to the oxygen vacancy diffusion controlling the growth of a dense zirconia layer;
- in some parts of the zirconia/oxide interface, the nitrogen concentration is sufficiently high (see stability phases diagram in section 2) to initiate a reaction with the metallic phase (in fact α-Zr(O) phase) and form zirconium nitride with outward growth, resulting in voids near the reacting interfaces;
- these voids and the mechanical stresses associated with the outward growth of the nitride phase are very probably at the origin of the cracks, which initiate the acceleration of the mass gain because of a loss of the protective character of the initially dense zirconia layer. The cracks appear at random on the sample surface, such as do the nuclei in a gas-solid chemical reaction, the number of attacked regions per unit of time and surface area being characterized by a "nucleation frequency" depending on the local thermodynamical variables (temperature, concentrations in nitrogen and oxygen, mechanical stresses, etc.). Such an analogy between cracks and nucleation offers the opportunity to build kinetic models of accelerated corrosion based on nucleation and growth models used in the kinetic analysis of solid-gas reaction as previously proposed by Tupin and al. [29] and Coindreau and al. [1]. In the conditions chosen for this study, the "nucleation frequency" of the cracking process appears to be strongly influenced by the oxygen and nitrogen partial pressures as shown in Fig. 11 and Fig. 12. Effectively, the low partial pressures conditions favour cracking compared to the high partial pressures conditions;
- once the first crack (nucleus) appeared, rigorously the mass gain is due to both contributions of the growth of the zirconia dense layer in the still unattacked regions of the sample and, of the accelerated corrosion process (growth) occurring in the attacked regions, whose number may increase significantly with time. As far as the number of attacked regions increases, the first contribution becomes negligible compared to the second one. The minimum observed on the rate curves versus time and so-called "kinetic

transition" is thus due to the minimum appearing in the sum of a decreasing and increasing functions of time and, is not necessarily characteristic of a particular event;

- the accelerated corrosion following the cracking process due to nitride (and/or oxynitride) precipitates formation can be explained by successive series of Zry-4 nitriding – nitride oxidation reactions due to fast diffusion of O_2 and N_2 through the highly porous corroded layer. The nitride oxidation reaction leads to highly porous zirconia (the important porosity comes from the molar volume discrepancies between zirconium nitride and zirconia) and release of gaseous nitrogen near to the oxide-metal interface. In the same way, nitriding of the α-Zr(O) phase releases oxygen near to the metal which probably explains inner regions with dense zirconia. As the presence of pores prevents formation of a protective oxide layer, the accelerated corrosion process continues until total degradation of the metal (metal oxidation according to an inward growth, incorporation of nitrogen into a very thin oxide layer, metal nitriding following an outward growth and oxidation of zirconium nitride precipitates).

5 Conclusion

Qualitative analyses presented in this paper provide useful information for the kinetic modelling of the accelerated corrosion in the post-transition stage. The reaction zones have been carefully examined after corrosion in low and high partial pressures of O_2-N_2 mixtures at 850°C. Regarding the role of both gases, it has been shown that the initiation of the accelerated corrosion is due to the nitriding of the metallic zirconium with outward growth, and that it may be uniform or localised according to oxygen and nitrogen concentrations in the reacting atmosphere. Work is in progress in order to put in an equation the kinetic rate in the post-transition stage on the basis of surface nucleation and growth models developed for chemical transformations of solid phases. But since such kinetic models rely on the steady-state approximation and on the existence of an elementary step controlling the growth process, it will be important for this highly complex reactive system (two reacting gases, many solid phases and interfaces to take into consideration) to verify that both assumptions are well established as long as the transformation proceeds. Otherwise, it it will be very difficult to establish a valuable kinetic modelling. However, the main difficulty would be to know, considering the three reactions that are possibly involved during corrosion in air (metal

oxidation, metal nitriding and zirconium nitride oxidation), what could be the rate-determining step during the post-transition stage.

The corresponding study will be the topic of a further article in the near future.

6 References

[1] O. Coindreau, C. Duriez, S. Ederli, *J. Nucl. Mater.* 2010, 405, 207-215.

[2] C. Duriez, T.Dupont, B. Schmet, F. Enoch, *J. Nucl. Mater.* 2008, 380, 30-45.

[3] C. Duriez, M. Steinbrück, D. Ohai, T. Meleg, J. Birchley, T. Haste, *Nucl. Eng. Des.* 2009, 239, 244-253.

[4] M. Steinbrück, *J. Nucl. Mater.* 2009, 392, 531-534.

[5] M. Steinbrück, M. Böttcher, *J. Nucl. Mater.* 2011, 414, 276-285.

[6] M. Steinbrück, *presented at HTCPM*, Les Embiez, France, 2012.

[7] J. Debuigne, *Ph.D. Thesis*, Faculté des sciences de l'université de Paris, 1966.

[8] E.B. Evans, N. Tsangarakis, H.B. Probst, N.J. Garibotti, *presented at the Metallurgical Society of AIME Symposium on High Temperature Gas-Metal Reactions in Mixed Environments*, 1972.

[9] C.J. Rosa, W.W. Smeltzer, *Z. Metallkde* 1980, 470-474.

[10] I. Idarraga, *Ph.D. Thesis*, Université de Grenoble, Grenoble, 2011.

[11] M. Steinbrück, M. Jung, *presented at ICAPP (International Congress on Advances in Nuclear Power Plants)*, Nice, France, 2011.

[12] M. Lerch, *J. Mater. Sci. Lett.* 1996, 15, 2127-2129.

[13] I. Valov, J. Janek, *Solid State Ionics* 2006, 177, 1619-1624.

[14] I. Valov, *Ph.D. Thesis*, Justus-Liebig-University, Giessen, 2006.

[15] S. Gutzov, M. Lerch, *Ceram. Int.* 2007, 33, 147-150.

[16] N. Claussen, R. Wagner, L.J. Gauckler, G. Petzow, *J. Am. Ceram. Soc.* 1978, 61, 369-370.

[17] Y. Cheng, D.P. Thompson, J.*Am. Ceram. Soc.* 1991, 74, 1135-1138.

[18] Y. Cheng, D.P. Thompson, *J. Am. Ceram. Soc.* 1993, 76, 683-688.

[19] T.J. Chung, J.S Lee, D.Y. Kim, *J.Am. Ceram. Soc.* 2001, 84, 172-178.

[20] R. Collongues, J.C. Gilles, A.M. Lejus, M. Perez y Jorba, D. Michel, *Mat. Res. Bull.* 1967, 2, 837-848.

[21] M. Lerch, *J.Am. Ceram. Soc.* 1996, 79, 2641-2644.

[22] M. Lerch, F. Krumeich, R. Hock, *Solid State Ionics* 1997, 95, 87-93.

[23] M. Lerch, O. Rahäuser, *J. Mater. Sci.* 1997, 32, 1357-1363.

[24] M. Lerch, J. Janek, K.D. Becker, S. Berendts, H. Boysen, T. Bredow, R. Dronskowski, S.G. Ebbinghaus, M. Kilo, M.W. Lumey, M. Martin, C. Reimann, E. Schweda, I. Valov, H.D. Wiemhöfer, *Prog. Solid State Chem.* 2009, 37, 81-131.

[25] D.A. Dzivenko, *Ph.D. Thesis*, Technischen Universität Darmstadt, Darmstadt, 2009.

[26] M. Tupin, *Ph.D. Thesis*, Ecole Nationale Supérieure des Mines de Saint-Etienne, Saint-Etienne, 2002.

[27] M. Pijolat, F. Valdivieso, M. Soustelle, *Thermochim. Acta* 2005, 439, 86-93.

[28] M. Pijolat, M. Soustelle, *Thermochim. Acta* 2008, 478, 34-40.

[29] M. Tupin, F. Valdivieso, M. Pijolat, M. Soustelle, A. Frichet, P. Barberis, *Mater. Sci. Forum* 2004, 461-464, 139-146.

[30] T. Delachaux, *Ph.D. Thesis*, École Polytechnique Fédérale de Lausanne, Lausanne, 2003.

Figures

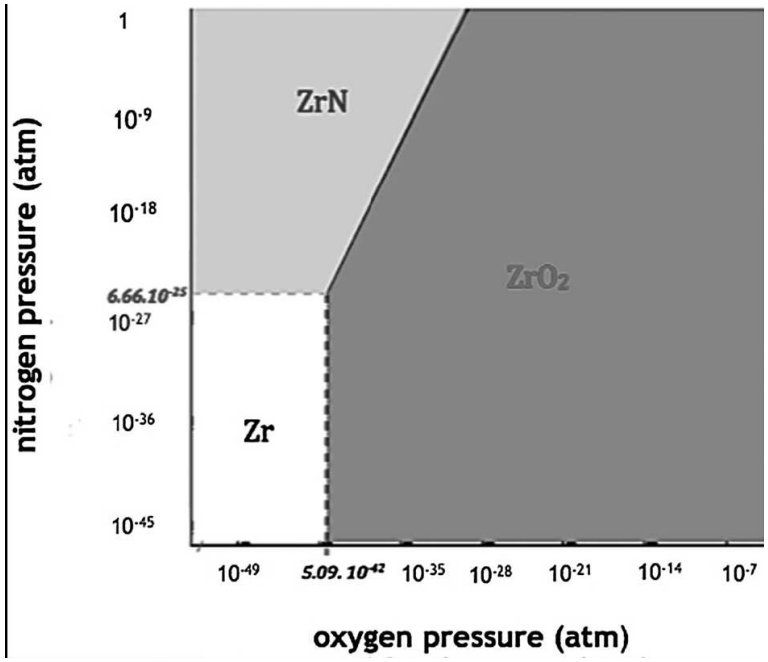

Figure 1 : Zr, ZrN, ZrO_2 stability diagram at 850 8C (1123 K)

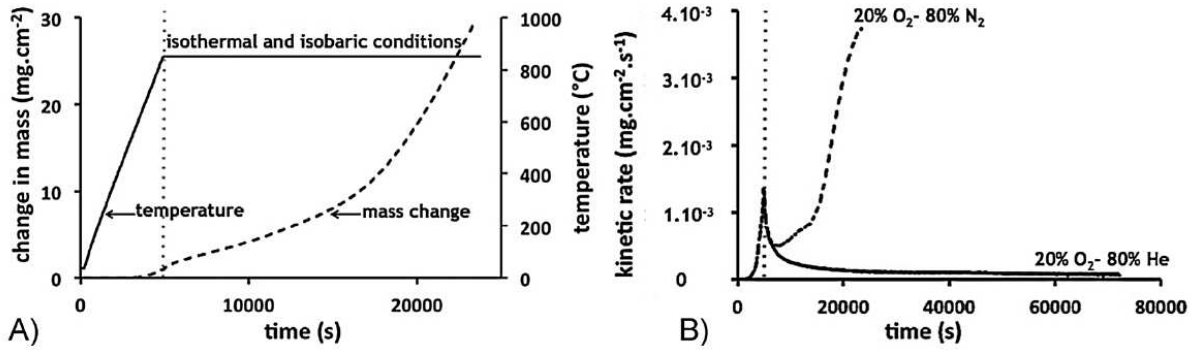

Figure 2 : (A) mass change in 20% O_2–80% N_2 as a function of time (hyphenated curve); (B) kinetic rate as a function of time in 20% O_2–80% N_2 (hyphenated curve) and in 20% O_2–80% He (full curve)

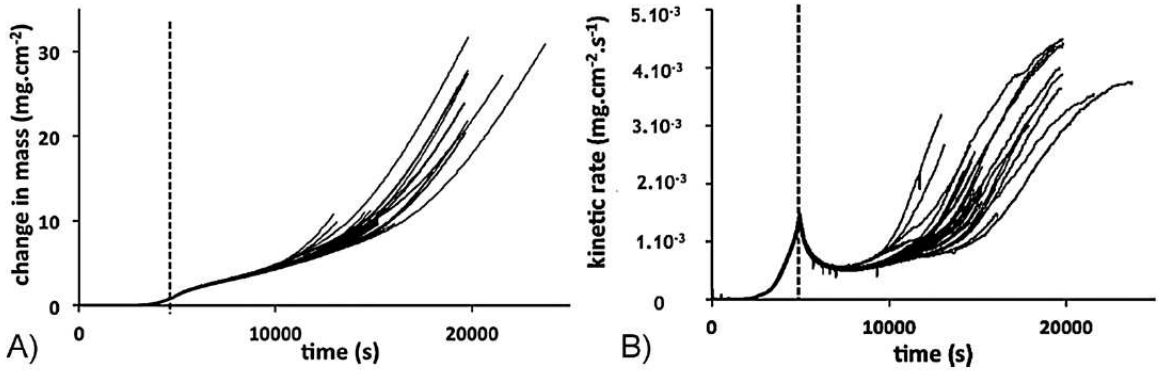

Figure 3 : Reproducibility during corrosion of Zry-4 in 20% O_2–80% N_2; (A) change in mass; (B) kinetic rate

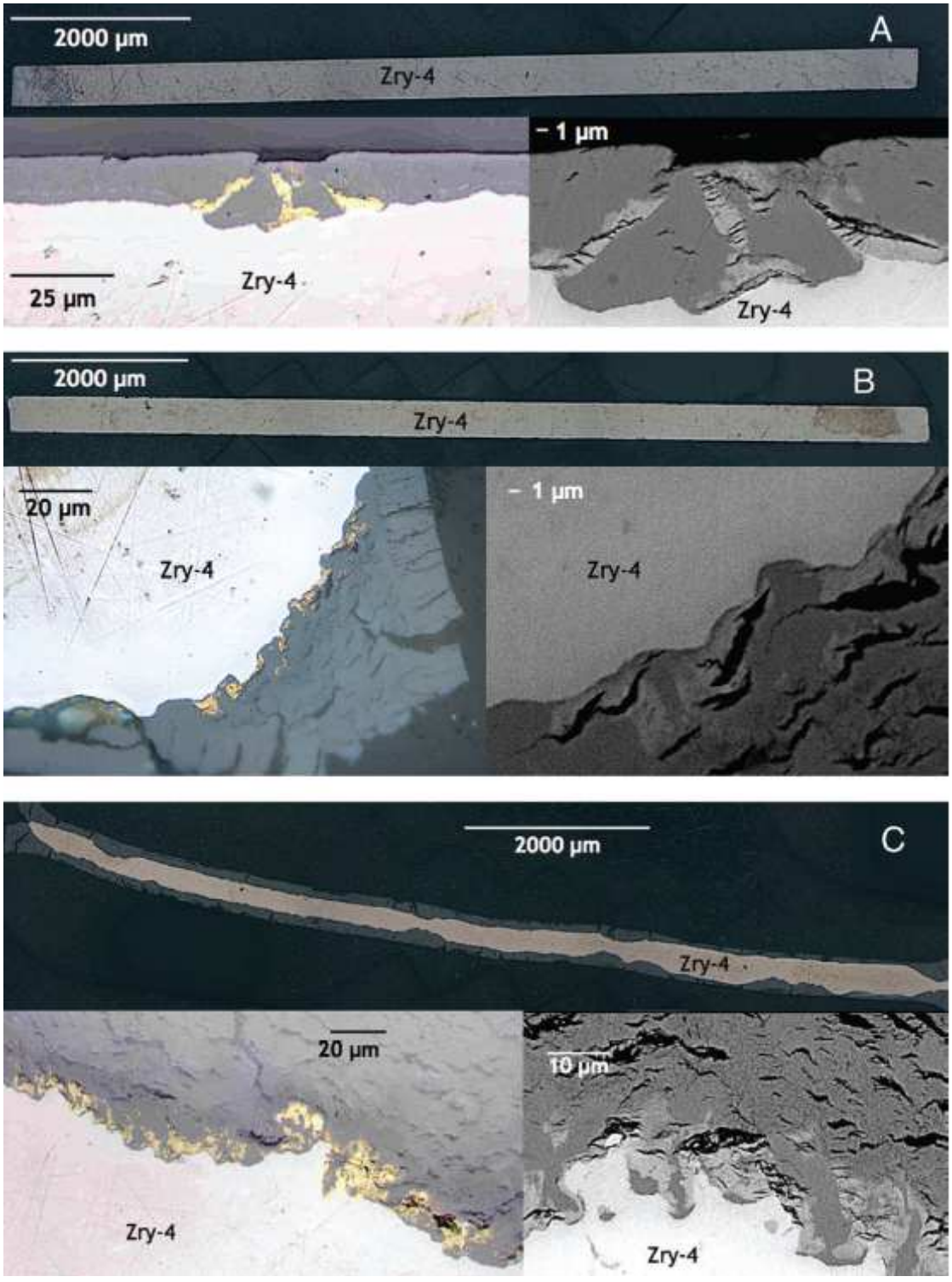

Figure 4: Zry-4 in 20% O_2–80% N_2 atmosphere during the pre-transition stage (A: mass gain of 1.76 mg/cm^2), at the kinetic transition (B: mass gain of 2.73 mg/cm^2), during the post-transition stage (C: mass gain of 15.76 mg/cm^2); top: global aspect (50 x magnification); bottom left: optical metallography (1000 x magnification); bottom right: SEM in backscattered electron mode (3000 x magnification for A and B, 1500 x magnification for C)

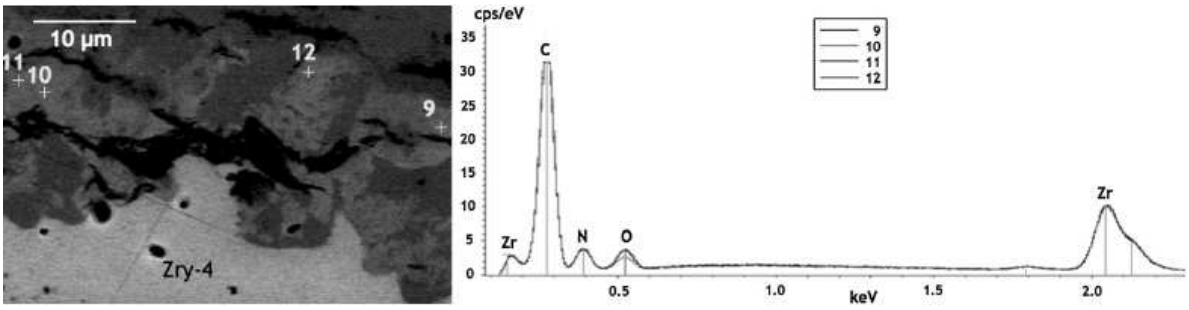

Figure 5 : Zry-4 in the post-transition stage; left: SEM (2000 x magnification) and the four analyzed zones (9, 10, 11, and 12); right: EDX-SDD spectrum

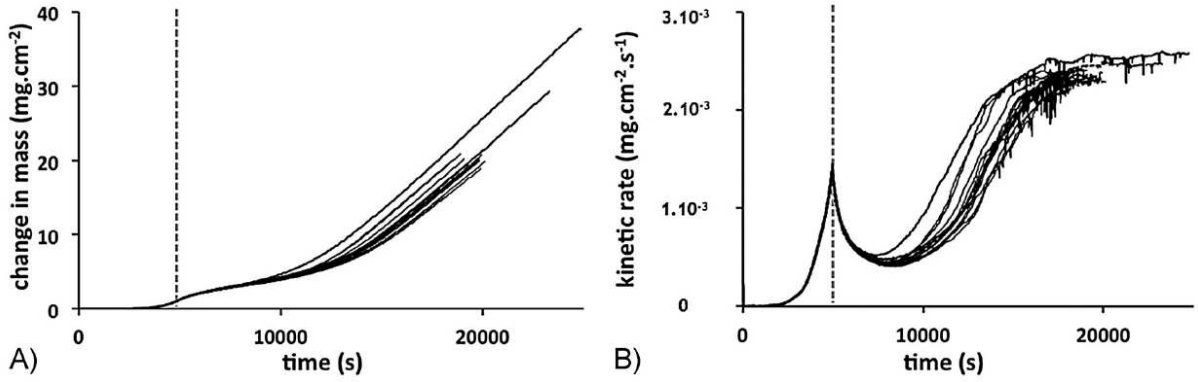

Figure 6 : Reproducibility during corrosion of Zry-4 in 5% O_2–5% N_2–90% He; (A) change in mass; (B) kinetic rate

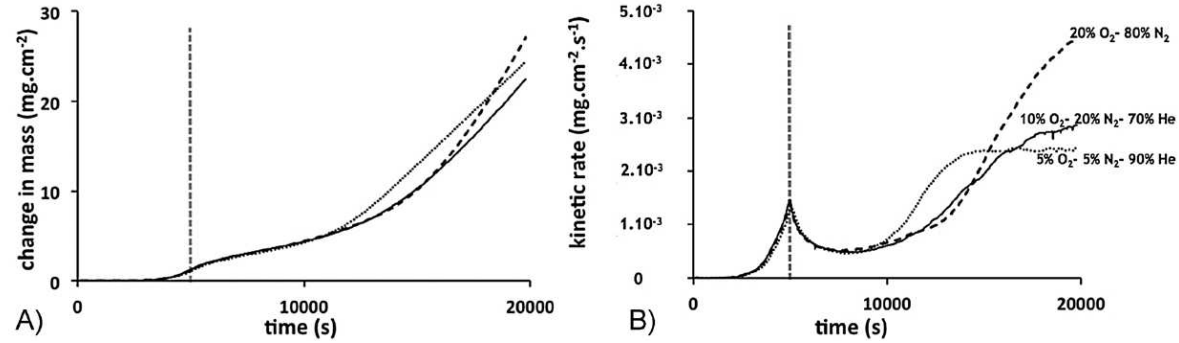

Figure 7 : Zry-4 in 20% O_2–80% N_2 atmosphere (hyphenated curve), in 5% O_2–5%N_2–90% He atmosphere (dotted curve), in 10% O_2–20%N_2–70% He atmosphere (full curve); (A) change in mass; (B) kinetic rate

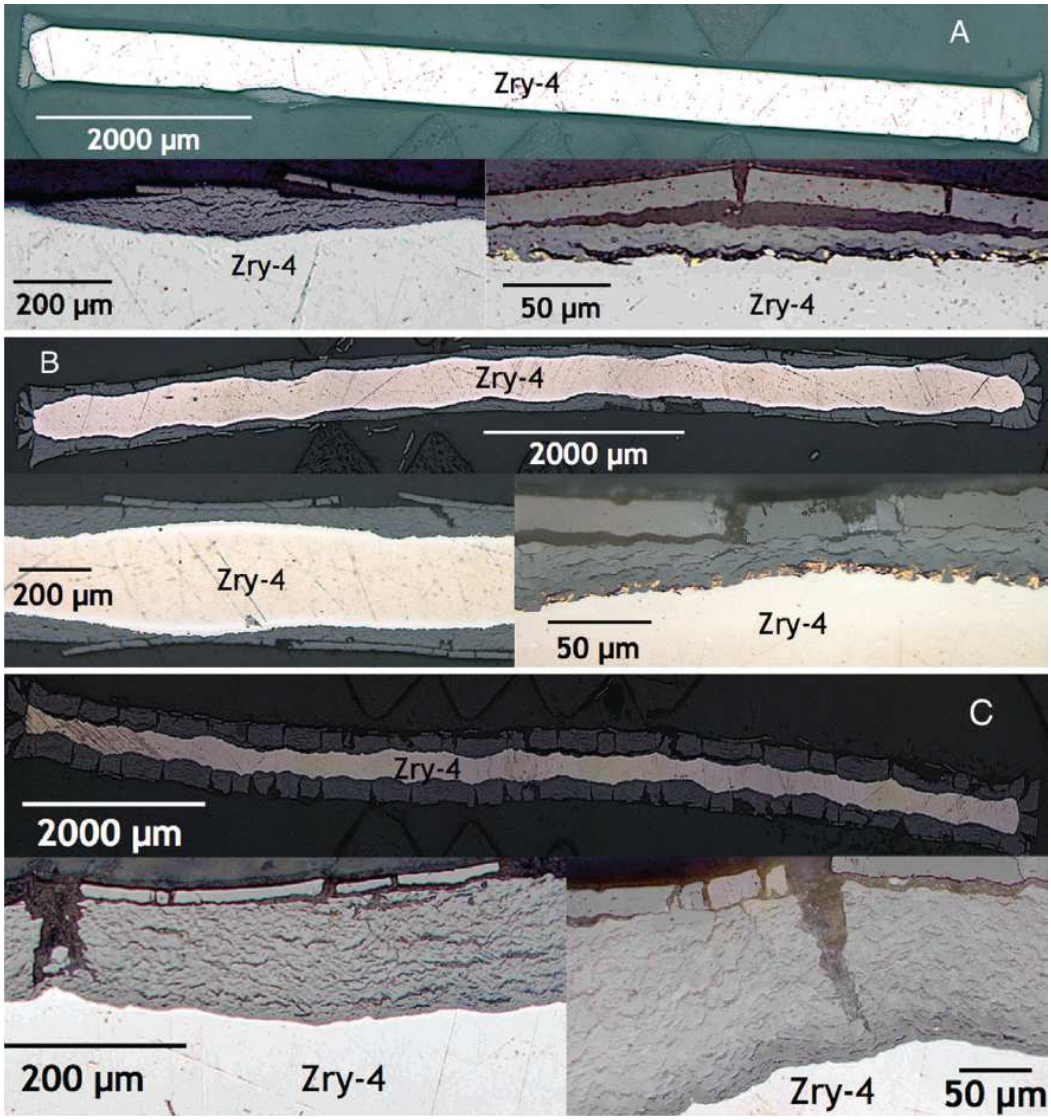

Figure 8 : Optical metallography of Zry-4 in 5% O_2–5% N_2–90% He atmosphere just after the kinetic transition (A: mass gain of 5 mg/cm^2), during the kinetic acceleration (B: mass gain of 10.2 mg/cm^2), when the kinetic rate is constant (C: mass gain of 35 mg/cm^2); top: global aspect (50 x magnification); bottom left: 200 x magnification; bottom right: 500 x magnification

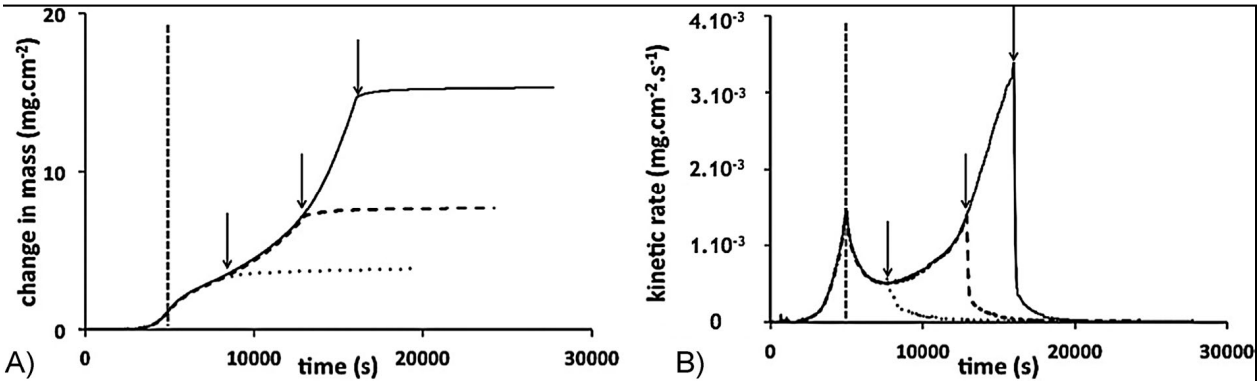

Figure 9 : Zry-4 in 20% O_2–80% N_2 atmosphere, switch to inert atmosphere (arrows): at 2.55 mg/cm^2 (dotted curve), at 6.45 mg/cm^2 (hyphenated curve) and at 13.95 mg/cm^2 (full curve); (A) change in mass; (B) kinetic rate

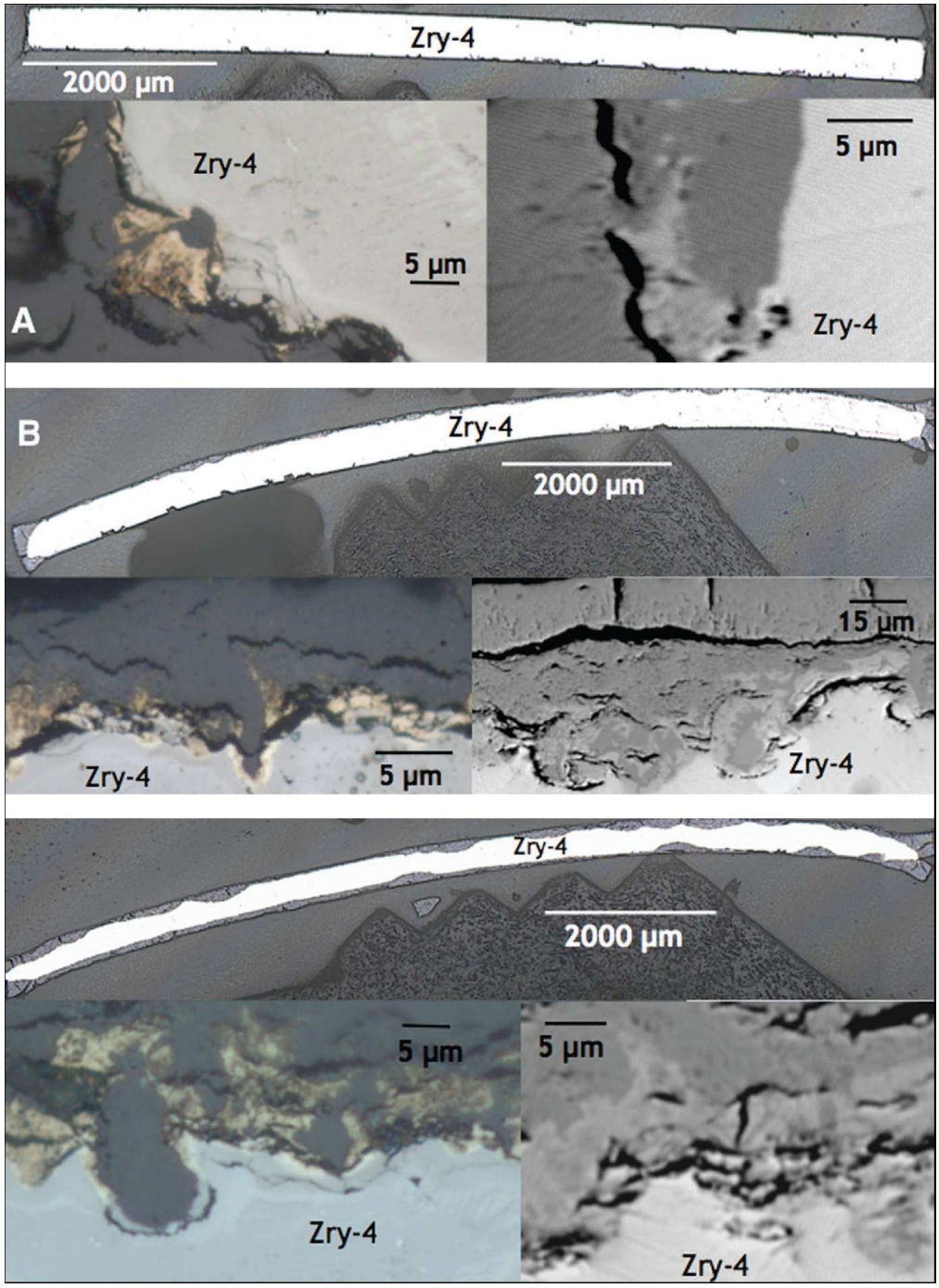

Figure 10 : Zry-4 in 20% O_2–80% N_2 atmosphere, switch over to inert atmosphere at 2.55 mg/cm^2 (A), at 6.45 mg/cm^2 (B), and at 13.95 mg/cm^2 (C); top: global aspect (50 x magnification); bottom left: optical metallography (1000 x magnification); bottom right: SEM (2500 x magnification for A and C, 1000 x magnification for B)